Bioinspired Soft Bendable Peristaltic Pump Exploiting Ballooning for High Volume Throughput

Leone Costi, *Student Member, IEEE*, Josephine Hughes, *Member, IEEE*, John Biggins, and Fumiya Iida, *Senior Member, IEEE*

***Abstract*—Interest in bioinspired peristaltic pumps has grown in popularity among the scientific community in the last decade thanks to their extreme flexibility and their intrinsic compliance. In this paper, we propose a soft peristaltic pump exploiting ballooning. Our aim is to promote and propel forward the ballooned region by controlling the air pressure between the balloon and an external flexible containment tube, to achieve a peristaltic pumping motion with a simple design and using only one control signal. This paper describes the implementation of the pump and the inlet-pump-outlet system, provides an analytical model to predict the pump performance, and showcases experimental results. We also implement a computer simulation to further characterize the device. We show that it is possible to achieve high volumetric flow rates, up to 4.4 mL/s, with only a single control signal, paving the way for more flexible and easy to manufacture peristaltic pumps.**

***Index Terms*—Soft robotics, bioinspired robotics, mechanical systems, pumps, pneumatic actuators.**

I. Introduction

ROBOTICS has become integral to everyday life in modern society, but rigid robots show strong limitations in compliance, safety, and flexibility. This is where soft robotics excels, using stretchable and flexible materials as structural elements and actuators [1], [2]. Considering the sub-domain of peristaltic pumps, rigid pumps achieve the characteristic peristaltic motion by temporally crimping the tube with rollers [3], potentially cutting and damaging the tube if the medium contains solid particles. Conversely, soft pumps reproduce the peristaltic motion observed in biological systems [4] by understanding and replicating motion primitives observed in nature [5], achieving high compliance and good flexibility. Soft peristaltic pumps generate pulsatile flow thanks to a travelling peristaltic contraction wave, unlikely Liebau pumps that exploit a periodic but spatially static contraction [6]. The bending capability of such devices makes them suitable for performing actuation in narrow and tight spaces with obstacles, such as medical applications [7].

The actuation technologies exploited so far for peristaltic actuation are dielectric active elastomers (DAEs) [8], [9], [10], magnetic actuators (MAs), shape memory alloys (SMAs) [11], [12] and pneumatic artificial muscles (PAMs) [13], [14], [15]. Among these, DAEs and MAs are able to achieve high frequencies, up to 10 Hz, but the limited stroke is unable to provide high flow rates. Instead, PAMs showcase the best flow rate, from few mL/s up to 75 mL/s, thanks to a modular architecture bioinspired from the small intestine [16], [17], [18]. Although powerful, this solution shows extreme complexity in fabrication, control, and scalability, due to the modular design: each module needs to be connected to the air supply and controlled independently. Overall, state-of-the-art pumps show either a low flow rate or extreme complexity and limited flexibility due to the wiring.

In this work, we propose a non-modular design exploiting and controlling the buckling of an elastomeric balloon, known as ballooning. Ballooning is the phenomenon by which balloons, when inflated, rapidly create a localized completely expanded region, with little deformation of the rest of the structure [19]. In this configuration, all possible positions of the inflated regions are energetically equivalent [19], [20]. Our aim is to promote ballooning and then propel the inflated region forward, after which reversing the buckling at the end of the pump to create a peristaltic pumping motion that can then be cycled. However, controlling buckling is a complex and problematic task, since it is an unstable phenomenon very sensitive to any change in geometry or load [21], [22], [23]. Moreover, we want to achieve this motion using as few control signals as possible, in order to simplify the design of the pump and avoid the drawbacks of modular solutions. Finally, we want a model that allows the optimization of design and control parameters. We propose using an external flexible tube to constrain the balloon. If the inner diameter of the tube is smaller than the diameter of the inflated balloon, the ballooning would seal the tube and create two distinct regions: one proximal, between the inlet and the inflated region, and the other distal,

Manuscript received 15 March 2022; revised 17 May 2022 and 20 June 2022; accepted 15 July 2022. Date of publication 20 July 2022; date of current version 17 August 2022. This article was recommended for publication by Associate Editor A. Casals and Editor P. Dario upon evaluation of the reviewers' comments. This work was supported in part by the SMART Project, European Union's Horizon 2020 Research and Innovation through the Marie Sklodowska-Curie Grant under Agreement 860108, and in part by the UKRI Future Leaders Fellowship under Grant 658MR/S017186/1. *(Corresponding author: Leone Costi.)*

Leone Costi, John Biggins, and Fumiya Iida are with the Department of Engineering, University of Cambridge, Cambridge CB2 1TN, U.K. (e-mail: lc830@cam.ac.uk; fi224@cam.ac.uk.com).

Josephine Hughes is with the Department of Engineering, University of Cambridge, Cambridge CB2 1TN, U.K., and also with the Mechanical Engineering, Swiss Federal Institute of Technology in Lausanne, 1015 Lausanne, Switzerland.

Digital Object Identifier 10.1109/TMRB.2022.3192763

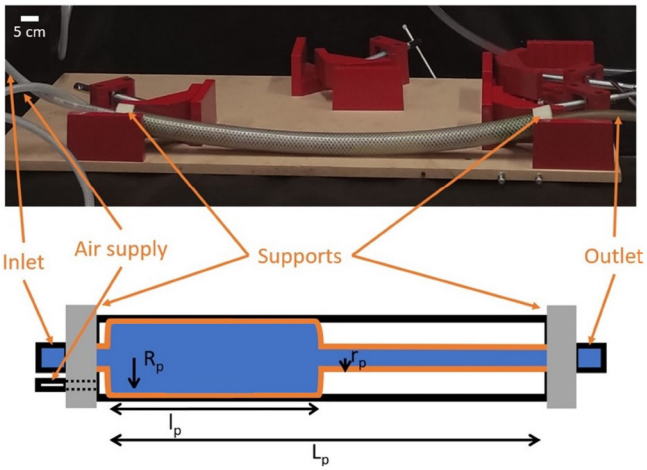

Fig. 1. Experimental pump implementation showing inlet, outlet and air supply. The parameters in figure are $L_p = 45\ cm$, $l_p = 20\ cm$, $R_p = 0.63\ cm$ and $r_p = 0.2\ cm$.

between inflated region and outlet. Then, we can use a single control pressure signal on the proximal region to achieve the peristaltic motion, allowing on/off control to trigger pumping. Finally, by developing a mathematical model of the inlet-pump-outlet system, we aim to give an additional tool for designing soft pumps that exploit ballooning. In particular, our device is shown to achieve volumetric flow rates up to 4.4 mL/s, outperforming other single input systems. For the remainder of the manuscript, the volumetric flow rate is simply referred as flow rate. It is also able to operate up to 1 Hz, similarly to other examples in literature [12], [18]. In addition, it requires only one control signal, independently from the device's length. It is also demonstrated that considerable bending and twisting do not affect the pump's performance, making this solution optimal for applications in tight or winding spaces.

In the remainder of the paper, we present the material and methods, including a mathematical model of the device, in Section II, and the results in Section III.

II. Material and Methods

A. Pump Design and Fabrication

The proposed pump design consists of two main components: the balloon and the external tube. The balloon is kept in position inside the tube by two supports that also connect the balloon to the inlet and outlet tubes. The left support also provides the connection to the air supply from the pneumatic regulator so that the pressure between balloon and tube can be regulated and controlled (see Fig. 1).

For the fabrication, we used a $2.2 \cdot 10^{-3}$ cm thick natural latex balloon (*Pengxiaomei, Modelling Balloons*) [24], [25] and a PET-PVC external tube (*RS Components, 368-0233*) [26]. The external tube's length is 45 cm to match the partially inflated balloon's length, and its internal diameter is 0.126 cm to ensure a tight junction with the balloon. The inlet and outlet supports have been 3D printed with ABS to fit the ends of the pump and host the needed connections. All the components are assembled together by hand. To achieve spontaneous ballooning, the

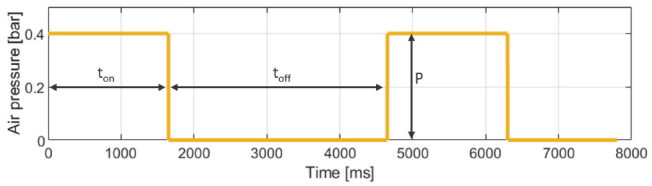

Fig. 2. Control pressure signal used to create peristaltic motions. P is the high pressure value of the square wave, and t_{on} and t_{off} are the activation and rest time, respectively.

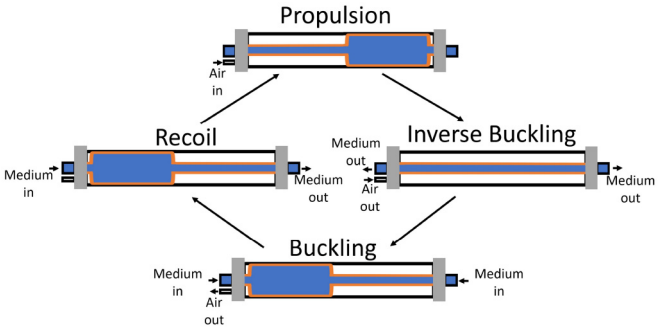

Fig. 3. Schematics of the pumping cycle and its four phases. Propulsion and inverse buckling happen during the activation of the pneumatic regulator, while buckling and recoil happen in the rest time.

device needs to be placed at a lower level than the water source connected to the inlet, so that the fluid pressure inside the balloon can trigger the buckling, and the balloon presents itself with an inflated region. Experimentally, it has been observed that placing the device at a distance $d_{max} = 160\ cm$ below the water source produces a spontaneously inflated region of length $l_p = 20\ cm$. This phenomenon is more likely to happen in the proximal section because of balloons' imperfections.

The control of the pump is open-loop and the control signal used to achieve peristaltic motion is a square pressure wave between balloon and tube, supplied by the pneumatic regulator. The three tunable parameters are the maximum pressure P and the activation and rest time, t_{on} and t_{off} respectively (see Fig. 2).

The pumping cycle can be divided into four parts: recoil, inverse buckling, propulsion, and buckling (see Fig. 3). Buckling and recoil happen when the pressure between the balloon and the external tube is at the atmospheric level: buckling happens when the pneumatic regulator is switched off, due to the differential pressure between inside and outside the balloon, whereas recoil is the passive flow from inlet to outlet, due to a lack of pressure in the outlet following the ballooning. Conversely, propulsion and inverse buckling happen when the pneumatic regulator is switched on. The buckled balloon divides the external tube is two regions, one proximal and one distal: only the proximal is pressurized since the regulator is connected on the inlet side, resulting in a force propelling the inflated region forward.

B. Setup

Once the pump is assembled, it is connected to the inlet and the outlet tubes, which connect the pump with both source

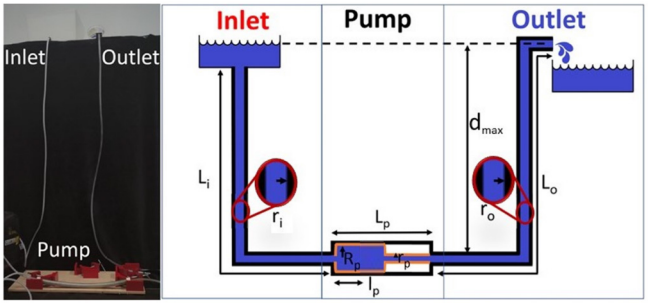

Fig. 4. Implementation and schematics of the set-up used to test the performance of the pump. $L_i = L_o = 300\ cm$, $r_i = r_o = 0.24\ cm$, $d_{max} = 160\ cm$, $L_p = 45\ cm$, $l_p = 20\ cm$, $r_p = 0.2\ cm$ and $R_p = 0.63\ cm$.

and target. The left support is also connected to the pneumatic regulator, which uses an air compressor operating at 10 *bar* as a source. The pneumatic regulator is controlled with Arduino UNO to achieve the square pressure wave. The pump is kept at a distance d_{max} below the fluid source and the target reservoir. Fig. 4 shows the experimental set-up and a corresponding schematic.

C. Mathematical Model

In this section, a mathematical model of the overall system is proposed in order to predict the performance as a function of the square pressure wave's parameters t_{on} and t_{off}. The following demonstration is divided into the four phases of the pumping cycle: recoil, inverse buckling, propulsion, and buckling. Since the buckling is a much faster phenomenon than recoil or propulsion, both the buckling and the inverse buckling will be considered instantaneous. All pressure values are referred to as gauge pressure.

1) Buckling: When the regulator switches off, the fluid's pressure $\rho g d_{max}$ (where ρ is the density of the inner fluid and g is the gravitational acceleration) causes ballooning, creating an inflated region that is filled with water from both outlet and inlet (see Fig. 5 a and b). Assuming that this phase happens instantly, it is supposed that the volume of water introduced in the pump $V_p = l_p \pi (R_p^2 - r_p^2)$ is provided by inlet and outlet depending on their distance from the middle point of the inflated region:

$$\begin{cases} V_{o1} = V_p \frac{L_{i1}}{L_{i1}+L_{o1}} \\ V_{i1} = V_p \frac{L_{o1}}{L_{i1}+L_{o1}} \end{cases} \tag{1}$$

where V_{o1} and V_{i1} are the volume of fluid provided by the outlet and the inlet, respectively, L_{i1} is the length of the inlet tube plus the distance from the start of the pump until the center of the inflated region and L_{o1} is the length of the outlet tube plus the remaining length of the pump, at this specific phase. The index 1 is used to indicate the first phase: buckling. Then, it is possible to compute the height $d_0 = \frac{V_{o1}}{\pi r_o^2}$, which is the starting point of the recoil.

2) Recoil: The recoil describes how the fluid level of the outlet raises to match the inlet. During this phase the distance d below the level of the fluid decreases as the outlet water level reaches the inlet's level (see Fig. 5 c and d). To describe the behaviour of the fluid, we compute the Reynolds number corresponding to the highest achieved flow rate of 4.4 mL/s (see Section III-D). Using the simplified formula for a flow in a pipe [27], we obtain a maximum Reynolds number of 1100, well below the 2300 transition threshold from laminar to turbulent. Because of the laminar nature of the flow, we can use Poiseuille's law to describe its dynamics. Nevertheless, in the proposed system the distance $d(t)$ is a function of the velocity of the fluid at the orifice, $v(t)$, leading to the following set of equations:

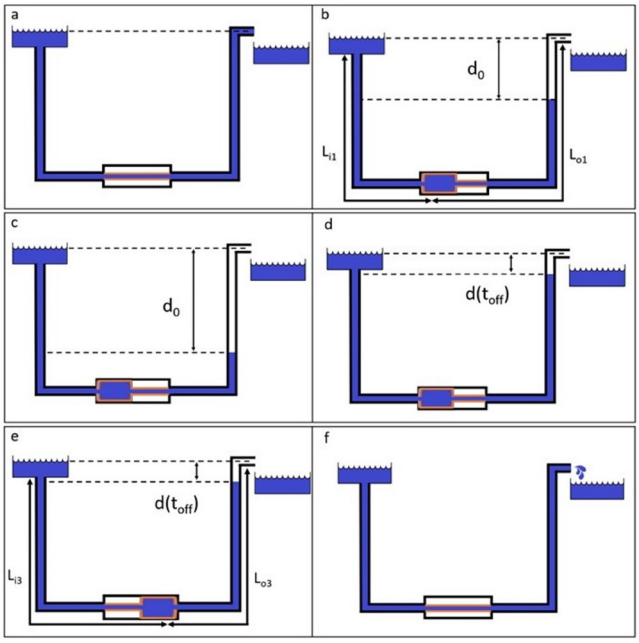

Fig. 5. Schematics of (a) before and (b) after the onset of the inverse buckling, (c) at the beginning and (d) at the end of the recoil, and (e) before and (f) after the onset of the buckling.

$$\begin{cases} v(t) = \frac{\rho g d(t) r_{eff}^2}{8\eta(L_i+Lo+Lp-d(t))} \\ d(t) = d_0 - \int_0^t v(x)\,dx \end{cases} \tag{2}$$

where η is the viscosity of the fluid and r_{eff} is the effective radius of the conduct computed as follows:

$$r_{eff} = \frac{r_i L_i + r_o L_o + R_p(L_p - l_p) + r_p l_p}{L_i + L_p + L_o} \tag{3}$$

Assuming that $L_i + Lo + Lp - d(t) \approx L_i + Lo + Lp$ and solving for $d(t)$, we obtain:

$$\begin{cases} d(t) = d_0 e^{-At} \\ A = \frac{\rho g r_{eff}^2}{\eta(L_i+Lo+Lp)} \end{cases} \tag{4}$$

Finally, we can compute the volume of fluid that is still needed to completely fill the outlet tube at the end of the recoil as $V_{empty} = \pi r_o^2 d(t_{off})$.

3) Inverse Buckling: This phase is the only one in which we have a net positive flow rate going into the receiving container (see Fig. 5 e and f). The total volume of water ejected is $V_{tot} = V_{o3} + V_{reb}$, where the first term is due to the inverse buckling and the second one is due to the rebound of the balloon itself after.

Following the same assumption of the buckling phase and correcting the outlet volume by the volume V_{empty} obtained

during the recoil phase, it is possible to compute the volume of water ejected by inverse buckling as follows:

$$\begin{cases} V_{o3} = V_p \frac{L_{i3}}{L_{i3}+L_{o3}-d(t_{off})} - V_{empty} \\ V_{i3} = V_p \frac{L_{o3}-d(t_{off})}{L_{i3}+L_{o3}-d(t_{off})} \end{cases} \tag{5}$$

where V_p is the volume of fluid inside the balloon before buckling, V_{o3} and V_{i3} are the volume of fluid ejected in the outlet's and inlet's reservoirs, respectively, L_{i3} is the length of the inlet tube plus the distance from the start of the pump until the center of the inflated region and L_{o3} is the length of the outlet tube plus the remaining length of the pump, at this specific phase. The index 3 is used to indicate the third phase: inverse buckling. Note that the inverse buckling happens distally, whereas the buckling happens proximally.

The second contribution is due to the rebound of the balloon. When an instantaneous change in volume happens (i.e., inverse buckling), the volume between the balloon and the tube increases suddenly, thus decreasing the pressure. Simultaneously, the air compressor tries to bring the pressure back up while the balloon would start inflating due to the fluid pressure on the inside. Those two phenomena cause a rebound of the balloon and more fluid is ejected as a consequence. Given the complexity of this problem, an analytical formulation is not provided, and the effect of rebound is modelled as a Gaussian process and fit to the residual output volume V_{res} to as follows:

$$\begin{cases} F_{reb} = ae^{\left(\frac{t_{on}-b}{c}\right)^2} \\ V_{res} = V_{exp} - V_{o3} \end{cases} \tag{6}$$

where V_{exp} are the experimental recorded data and F_{reb} is the component of the total flow rate resulting from the pumped volume V_{reb}. The parameters a, b and c are selected using the Nelder-Mead simplex optimization algorithm [28] on the experimental data: $a = 3.01$ mL/s, $b = 1987$ ms and c=1623 ms. These parameters allow us to characterize further the rebound: a represents the maximum contribution to the flow rate, which is achieved for a value of t_{on} equal to b. Moreover, c is the characteristic time constant of the process, and describes how fast the contribution of the rebound on the flow rate decays with time.

4) Propulsion: Upon activation of the regulator, the airflow introduced pushes the inflated region of the balloon from the proximal region to the distal one, where the inverse buckling happens. In the experiments the needed time for this process has been measured to be $\tau = 500$ ms for a 0.4 bar air pressure. Taking into consideration this time delay, the average flow rate of the pump F can be predicted as follows:

$$F = \frac{V_{o3}(t_{off})u(t_{on}-\tau)}{t_{on}+t_{off}} + F_{reb}(t_{on}) \tag{7}$$

where $u(t)$ is the unit step function.

D. Experiments

When testing the pump, the main outcome considered is the average flow rate: the pump is activated for five cycles and the total volume of water is then divided by the time needed to complete the cycles. To check whether taking only five cycles could introduce some performance bias related to a start up transient, we tested 6 balloons over 50 cycles each, and such a test revealed a not statistically significant difference of 0.024 mL/s, with a paired t-test indicating a p-value of 0.96, between the average flow rate computed after 5 cycles and after 50 cycles (see Fig. 6). Note that this experimental protocol allows to easily compute the average flow rate, but cannot estimate the instantaneous flow rate, preventing further characterization of peak flow rate and flow's dynamics within a cycle.

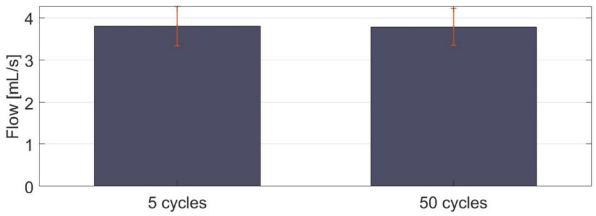

Fig. 6. Average flow of the device computed after 5 cycles and 50 cycles. The difference is found to be statistically non significant with a p-value of 0.96.

As a byproduct of this protocol, it is also possible to compute the efficiency e of the pumping mechanisms as follows:

$$e = \frac{P_0(t_{on}+t_{off})F}{PV_p} \tag{8}$$

where P_0 is the atmospheric pressure and P is the air pressure imposed by the pneumatic regulator. All experiments are run using water and every experiment is repeated 6 times with different balloons. Since the only control signal is a square pressure wave, the only 3 controllable parameters are P, t_{on}, and t_{off}. The parameters are initialized at 0.4 bar, 1650 ms and 7000 ms, respectively, and their effect on the average flow rate is characterized individually, based on experimental data: first t_{on}, then t_{off} and lastly P. The operation frequency of the pump can be computed as the inverse of the period ($t_{on}+t_{off}$). Next, the pump's performance in 5 configurations of increasing bending radius, up to 360 deg, is analyzed. Finally, the pump is also tested using coffee powder to simulate solid particles in the water.

E. MATLAB Simulation

Finally, the mathematical model described in Section II-C is implemented in a MATLAB simulation using *MATLAB 2020b* in order to exploit its potential. On one side, the model allows us to optimize multiple control parameters simultaneously and rapidly, using the model itself as objective function, avoiding the risk of local but not global optimal solution. On the other, it also allows us to optimize design parameters such as the pump dimensions without the need of a physical prototype, strongly reducing the overall design process.

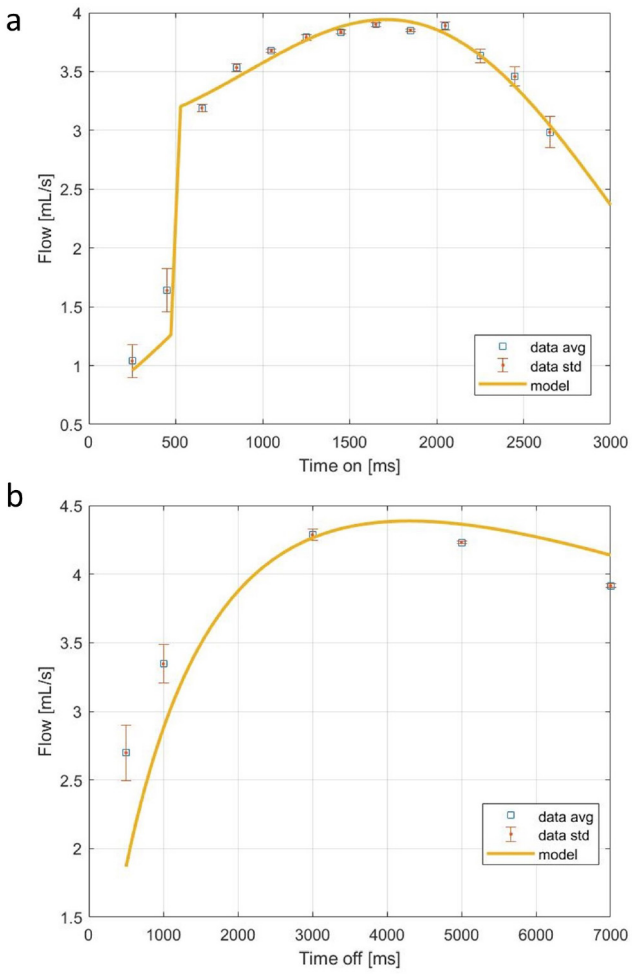

Fig. 7. Flow rate of the pump as a function of the activation and rest time, respectively. In (a) $t_{off} = 7000\ ms$ and in (b) $t_{on} = 1650\ ms$. Each tested value has been sampled 6 times using 6 different balloons.

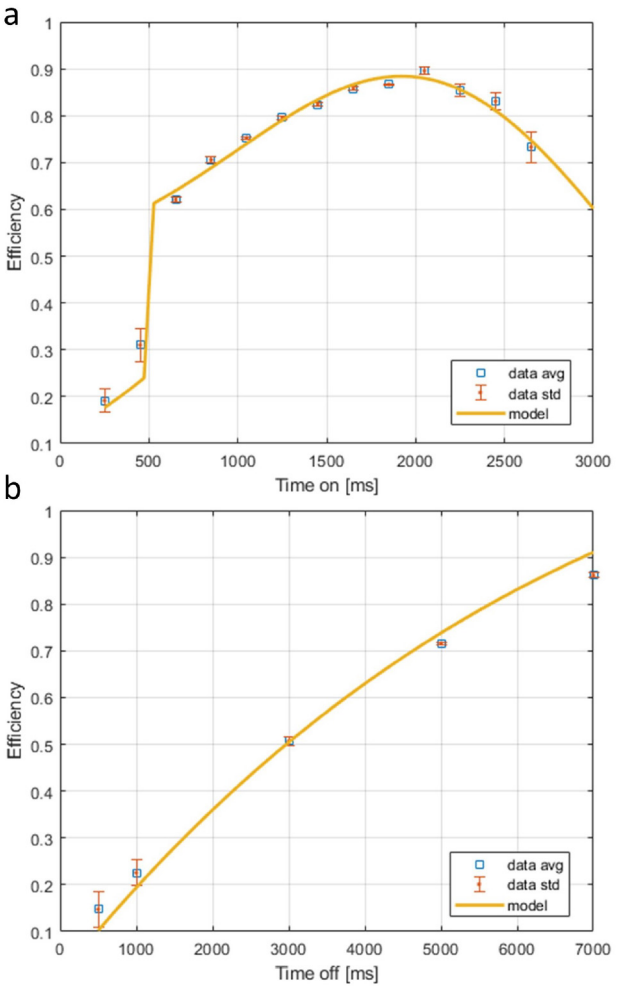

Fig. 8. Efficiency of the pump as a function of the activation and rest time, respectively. In (a) $t_{off} = 7000\ ms$ and in (b) $t_{on} = 1650\ ms$. Each tested value has been sampled 6 times using 6 different balloons.

III. Results

A. Control Signal Dependency: Time on and Off

First, keeping $P = 0.4\ bar$ and $t_{off} = 7000\ ms$, the pump has been tested and its performance has been evaluated as a function of t_{on} (see Fig. 7a). Next, fixing $t_{on} = 1650\ ms$, which corresponded to the maximum flow rate, the performance has been evaluated as a function of t_{off} (see Fig. 7b).

It can be noticed that the best performance is obtained for $t_{on} = 1650\ ms$ and $t_{off} = 3000\ ms$, but the pump is able to achieve a good performance up to a frequency of 1 Hz, with $t_{on} = 500\ ms$ and $t_{off} = 500\ ms$. If t_{on} is not enough to trigger the inverse buckling, there is a drop in performance due to the inflated region of the balloon not contributing to the ejected volume. It is also clear that the rest time needs to be sufficient for the fluid recoil to happen, otherwise, the majority of the ejected volume is wasted in the outlet tube and does not contribute to the pump's flow rate. Moreover, the proposed mathematical model is shown to enable accurate prediction of the pump's performance. Even if this is trivial for Fig. 7a, because of the fitting on the experimental data, it is not for 7b, proving that the model can grasp the effect of t_{off} on the pump's performance.

To further characterize the proposed pump design, Fig. 8 shows the efficiency of the pump as a function of t_{off} and t_{on}, computed according to equation 8. The results show that the two variables strongly affecting the efficiency are the average flow rate and the time off. Especially this last observation outlines the importance of the recoil phase: the longer t_{off} is, the smaller V_{empty} results, increasing significantly the efficiency of the system.

B. Control Signal Dependency: Pressure

Next, keeping constant the optimized parameters $t_{on} = 1650\ ms$ and $t_{off} = 3000\ ms$, the effect of the pressure's amplitude is investigated (see Fig. 9).

The bar chart shows that both low and high pressures result in a substantial decrease in performance, with statistical significance under a paired t-test. Analytically, increasing the operating pressure results in a lower τ and lower magnitude of the rebound output volume V_{reb}. With a pressure of 0.2 bar, the force exerted on the inflated region is not sufficient to propel it forward and to promote the inverse buckling, lowering the total volume of fluid ejected per cycle. On the other hand, high values of pressure are achieved by increasing the

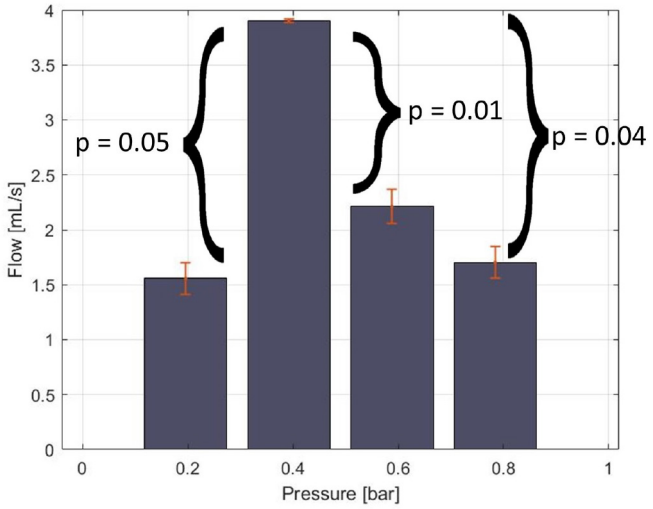

Fig. 9. Flow rate at different values of applied pressure, with $t_{on} = 1650\ ms$ and $t_{off} = 3000\ ms$. Each tested value has been sampled 6 times using 6 different balloons. The p-values of statistically significant differences are shown. Paired t-test has been used to compute statistical significance.

pneumatic regulator's airflow rate: this not only reduces the contribution of the rebound, but can result in the inflated region undergoing inverse buckling before reaching the end of the propulsion phase, as seen by visual inspection.

C. Performance Under Non-Ideal Conditions

To test the flexibility of the proposed pump design, the best operational parameters $P = 0.4\ bar$, $t_{on} = 1650\ ms$ and $t_{off} = 3000\ ms$ are tested while bending the pump in different configurations. Fig. 10 shows the relative average flow rate with respect to the unbent configuration and how the different orientations are achieved.

The results show that the effect of bending is limited at most to 11%, even in the presence of kinks, with no statistical significance under a paired t-test, thus the pump could be used in clustered and dynamic environments and could be bent around obstacles without extreme losses, making it suited for tasks in narrow spaces with obstacles to avoid, such as surgical theaters and healthcare facilities [29]. Next, to investigate the effect of solid particles in the medium, the device is tested pumping a slurry obtained by mixing 150 g of coffee powder and 4 L of water, with the same parameters. We run the experiments with both water and the mixture, and while pumping the latter the flow rate is only $0.6 \pm 0.2\%$ lower, with no statistical significance under a paired t-test, showing that the presence of the powder does not affect at all the performance.

D. MATLAB Simulation

Finally, the implemented MATLAB model was used to optimize t_{on} and t_{off} simultaneously, and to also compute the efficiency of the pump in such conditions (see Fig 11).

The results show us that to maximize the average flow rate we should work close to the minimum t_{on} that can provide complete propulsion: the maximum flow rate of 4.4 mL/s is obtained with $t_{on} = 500\ ms$ and $t_{off} = 1994\ ms$. Nevertheless,

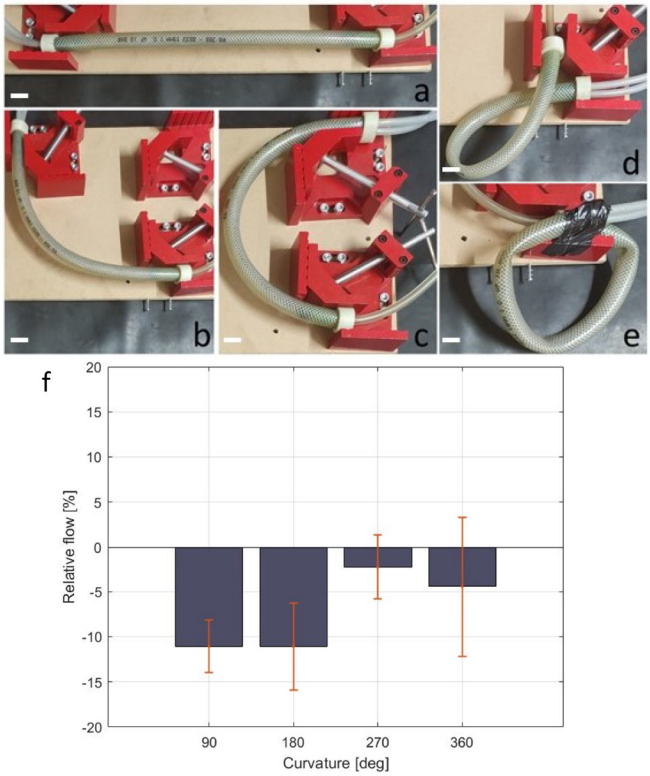

Fig. 10. Different pump configurations as the angle between inlet and outlet is increased: (a) 0 *deg*, (b) 90 *deg*, (c) 180 *deg*, (d) 270 *deg* and (e) 360 *deg*. Relative average flow rate with respect to the unbent configuration (f). The scale bar is 5 *cm*. Each tested configuration has been sampled 6 times using 6 different balloons.

because of the steep nature of this portion of the graph, a slightly lower but far more stable performance can be obtained at t_{on} around 2000 ms, provided that t_{off} is high enough to allow the recoil. Once more, t_{off} is shown to have an important effect on the efficiency on the pump, whereas the dependency by t_{on} is strongly dictated by the average flow, rather than directly by t_{on}.

Having a simulation of the performance allows us also to rapidly investigate the effects of the pump geometry without the need of physical prototypes. In turn, this leads to a faster optimization of the device, based on the analytical function described in Section II-C, depending on the final application's requirements. Fig. 12 shows the effect of changing length and diameter of the device.

It is clear how increasing the length of the pump would increase the performance, due to the higher distance between the initial and final position of the peristalsis. On the other hand, changing the diameter has limited effect. Note that the inner balloon has a maximum diameter of 30 mm when inflated without external constrains, thus we only considered such value as a maximum pump's diameter. Even in this case, the maximum performance, 8.4 mL/s is obtained in a very steep and unstable region of the graph, in clear contrast with the more stable regime corresponding to higher values for both the length and the diameter. Concerning the efficiency, the results show a strong dependency from the average flow rate, and overall low values, indicating how this

TABLE I
OVERVIEW OF BIOMIMETIC PERISTALTIC PUMPING SYSTEM UTILIZING DIFFERENT ACTUATION PRINCIPLES

Authors	Actuation principle	Inner diameter $[cm]$	Length $[cm]$	Control signals	flow rate $[\frac{mL}{s}]$	Frequency $[Hz]$
Bowers et al.[8]	Dielectric active elastomer	4	0.25	1	0.04	$3-4$
McCoul et al.[9]	Dielectric active elastomer	1.5	5	1	–	–
Lotz[10]	Dielectric active elastomer	0.1	3.5	1	1.8×10^{-4}	10
Fuhrer et al.[30]	Magnetic actuation	0.95	24	4	1.3	4
Miki et al.[11]	Shape memory alloy	1.8	3.5	2	$3-6$	0.33
Sun et al.[12]	Shape memory alloy	0.9	8	3	0.013	$0.1-2$
Suzuki et al.[16]	Pneumatic artificial muscle	3	23.5	5	33	$1.2-2$
Dirven et al.[14]	Pneumatic artificial muscle	1.8	20	12	$5-10$	–
Esser et al.[18]	Pneumatic artificial muscle	2	26.7	8	75	1.25
Our solution	Pneumatic buckling	2	45	1	$3-5$	$0.2-1$

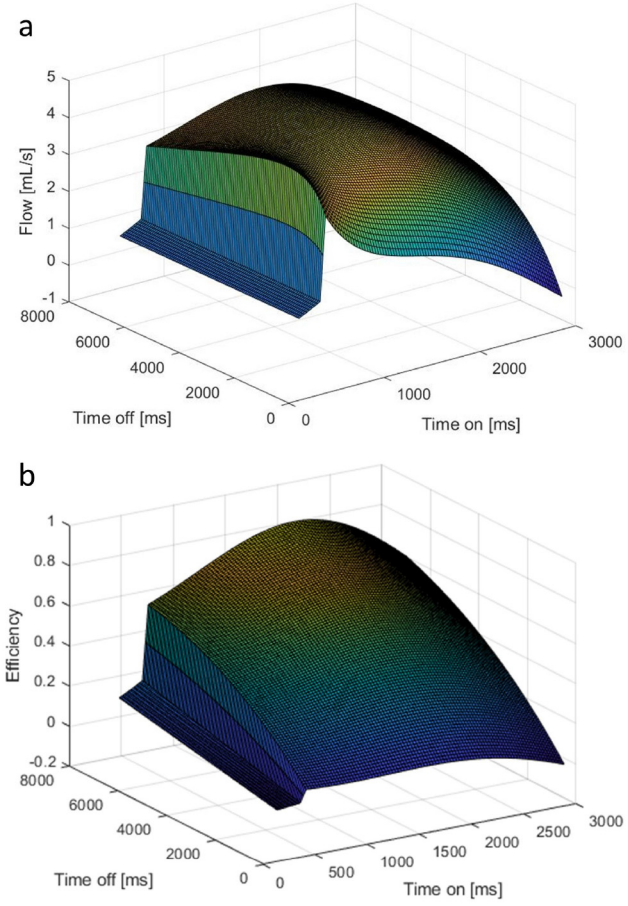

Fig. 11. Simulated flow rate (a) and simulated efficiency (b) as a function of t_{on} and t_{off}.

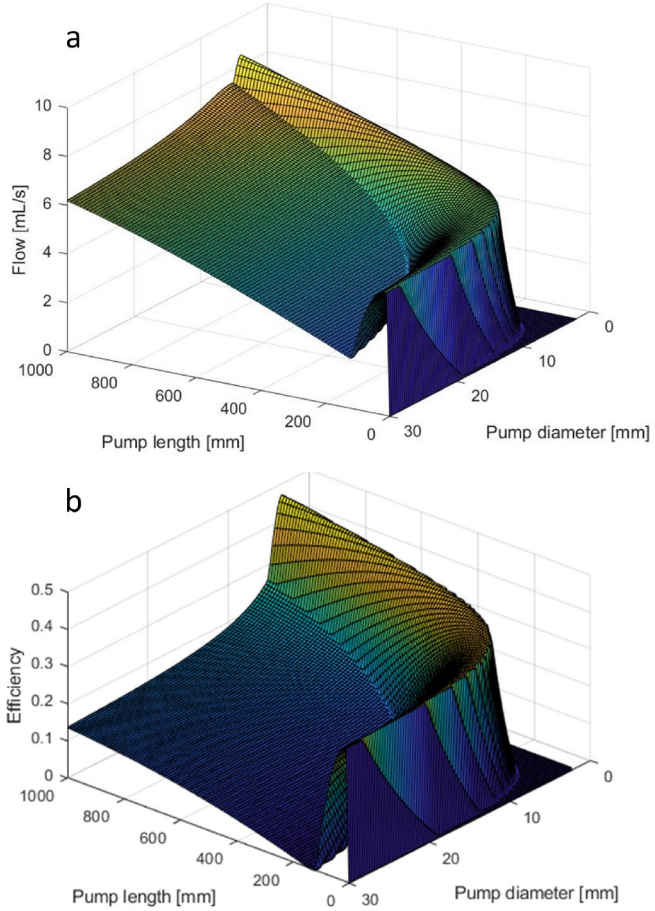

Fig. 12. Simulated flow rate (a) and simulated efficiency (b) as a function of pump's diameter and length.

choice of t_{on} and t_{off} showcases low efficiency at any selected geometry.

E. State-of-the-Art Comparison

When compared with other state-of-the-art biomimetic peristaltic soft pumps (see Table I), the proposed solution showcases a flow rate up to 4.4 *mL/s*, which is second only to modular PAMs. In addition, thanks to its non-modular design, the pump requires only one control signal, regardless of the pump's dimensions. However, the operating frequency of the proposed device is slightly lower than other state-of-the-art pumps, with a maximum of 1 *Hz*. Overall, the proposed device is shown to be a possible alternative to state-of-the-art peristaltic soft pumps. Moreover, avoiding all the supply wires characteristic of modular designs, the pump shows enhanced flexibility and steady performance when adding solid particles to the pumped medium.

IV. CONCLUSION

This work proposes an innovative strategy to achieve bioinspired peristaltic soft pumping: controlling the spontaneous buckling of a balloon filled with fluid. The pump is composed of a partially inflated single balloon containing the medium, and an external tube. To have a spontaneous inflated region,

the pump needs to be placed at a given distance below the level of the source and target reservoirs, but this constraint could be avoided by promoting the ballooning with a vacuum between the balloon and the external tube. The inflated region is moved using a single pneumatic regulator connected to the proximal end. By developing an analytical model and a MATLAB simulation, it is possible to investigate and optimize multiple parameters simultaneously, both for the control signal and the pump's design parameter, in order to maximize the average flow rate. The effects of amplitude, activation time, and rest time on the flow rate have been experimentally analyzed to provide a complete characterization, showcasing a maximum flow rate of 4.4 mL/s at a frequency of 0.4 Hz. Moreover, when tested in bent configurations and using different media, the device's average flow rate decreased at most by 11%. However, the flow rate strongly decreases above 1 Hz, due to failed propulsion and recoil's time scale. When compared with state-of-the-art soft peristaltic pumps, our approach is shown to have a greater flow rate than the other single input systems, second only to complex modular designs. Unlike the other pneumatic solutions in literature, the proposed pump is not modular, thus the length of the pump itself does not affect the fabrication nor the number of control signals needed to operate it. In summary, buckling provides many advantages to the pumping mechanism, enabling many novel functionalities and state-of-the-art performance. However, we acknowledge that our experimental setup allowed only the characterization of the average flow rate, and we endorse future studies on the analysis of the instantaneous flow rate. Future work could also include the parallel implementation of different balloons pumping different media, even non-Newtonian, and the systematic introduction of weak points to better control and stabilize the buckling.

REFERENCES

[1] J. Walker *et al.*, "Soft robotics: A review of recent developments of pneumatic soft actuators," *Actuators*, vol. 9, no. 1, p. 3, 2020.

[2] S. Kim, C. Laschi, and B. Trimmer, "Soft robotics: A bioinspired evolution in robotics," *Trends Biotechnol.*, vol. 31, no. 5, pp. 287–294, 2013.

[3] J. Klespitz and L. Kovács, "Peristaltic pumps—A review on working and control possibilities," in *Proc. IEEE 12th Int. Symp. Appl. Mach. Intell. Inf. (SAMI)*, 2014, pp. 191–194.

[4] S. Vogel, "Living in a physical world X. Pumping fluids through conduits," *J. Biosci.*, vol. 32, no. 2, pp. 207–222, 2007.

[5] D. Bach, F. Schmich, T. Masselter, and T. Speck, "A review of selected pumping systems in nature and engineering - potential biomimetic concepts for improving displacement pumps and pulsation damping," *Bioinspiration Biomimetics*, vol. 10, no. 5, 2015, Art. no. 051001.

[6] N. Sarvazyan, "Building valveless impedance pumps from biological components: Progress and challenges," *Front. Physiol.*, vol. 12, pp. 1–13, Jan. 2022.

[7] F. Esser, T. Masselter, and T. Speck, "Silent pumpers: A comparative topical overview of the peristaltic pumping principle in living nature, engineering, and Biomimetics," *Adv. Intell. Syst.*, vol. 1, no. 2, 2019, Art. no. 1900009.

[8] A. E. Bowers, J. M. Rossiter, P. J. Walters, and I. A. Ieropoulos, "Dielectric elastomer pump for artificial organisms," in *Proc. Electroactive Polym. Actuators Devices (EAPAD)*, vol. 7976, Mar. 2011, Art. no. 797629.

[9] D. McCoul and Q. Pei, "Tubular dielectric elastomer actuator for active fluidic control," *Smart Mater. Struct.*, vol. 24, no. 10, 2015, Art. no. 105016.

[10] P. Lotz, M. Matysek, and H. F. Schlaak, "Peristaltic pump made of dielectric elastomer actuators," in *Proc. Electroactive Polym. Actuators Devices (EAPAD)*, vol. 7287, Apr. 2009, Art. no. 72872D.

[11] H. Miki *et al.*, "Artificial-esophagus with peristaltic motion using shape memory alloy," *Int. J. Appl. Electromagn. Mech.*, vol. 33, nos. 1–2, pp. 705–711, 2010.

[12] X. Sun, Y. Hao, S. Guo, X. Ye, and X. Yan, "The development of a new type of compound peristaltic micropump," in *Proc. IEEE Int. Conf. Robot. Biomimetics ROBIO*, 2009, pp. 698–702.

[13] F. J. Chen, S. Dirven, W. L. Xu, and X. N. Li, "Soft actuator mimicking human esophageal peristalsis for a swallowing robot," *IEEE/ASME Trans. Mechatronics*, vol. 19, no. 4, pp. 1300–1308, Aug. 2014.

[14] S. Dirven, J. Allen, W. Xu, and L. K. Cheng, "Soft-robotic esophageal swallowing as a clinically-inspired bolus rheometry technique," *Meas. Sci. Technol.*, vol. 28, no. 3, 2017, Art. no. 035701.

[15] S. Yoshihama, S. Takano, Y. Yamada, T. Nakamura, and K. Kato, "Powder conveyance experiments with peristaltic conveyor using a pneumatic artificial muscle," in *Proc. IEEE/ASME Int. Conf. Adv. Intell. Mechatron. (AIM)*, Sep. 2016, pp. 1539–1544.

[16] T. Nakamura and K. Suzuki, "Development of a peristaltic pump based on bowel peristalsis using artificial rubber muscle," *Adv. Robot.*, vol. 25, no. 3, pp. 371–385, 2011.

[17] F. Esser, T. Steger, D. Bach, T. Masselter, and T. Speck, "Development of novel foam-based soft robotic ring actuators for a Biomimetic peristaltic pumping system," in *Proc. 6th Int. Conf. Living Mach.*, 2017, pp. 138–147.

[18] F. Esser, F. Krüger, T. Masselter, and T. Speck, "Characterization of biomimetic peristaltic pumping system based on flexible silicone soft robotic actuators as an alternative for technical pumps," in *Proc. 8th Int. Conf. Biomimetic Biohybrid Syst.*, Nara, Japan, Jul. 2019, pp. 101–113.

[19] A. Giudici and J. S. Biggins, "Ballooning, bulging and necking: An exact solution for longitudinal phase separation in elastic systems near a critical point," 2020, *arxiv.abs/2005.10535*.

[20] A. Rafsanjani, L. Jin, B. Deng, and K. Bertoldi, "Propagation of pop ups in kirigami shells," *Proc. Nat. Acad. Sci. USA*, vol. 116, no. 17, pp. 8200–8205, 2019.

[21] B. Deng, P. Wang, Q. He, V. Tournat, and K. Bertoldi, "Metamaterials with amplitude gaps for elastic solitons," *Nat. Commun.*, vol. 9, no. 1, pp. 1–8, 2018.

[22] B. Deng, Y. Zhang, Q. He, V. Tournat, P. Wang, and K. Bertoldi, "Propagation of elastic solitons in chains of pre-deformed beams," *New J. Phys.*, vol. 21, no. 7, 2019, Art. no. 073008.

[23] J. R. Raney, N. Nadkarni, C. Daraio, D. M. Kochmann, J. A. Lewis, and K. Bertoldi, "Stable propagation of mechanical signals in soft media using stored elastic energy," *Proc. Nat. Acad. Sci. USA*, vol. 113, no. 35, pp. 9722–9727, 2016.

[24] K. Genovese, L. Lamberti, and C. Pappalettere, "Mechanical characterization of hyperelastic materials with fringe projection and optimization techniques," *Opt. Lasers Eng.*, vol. 44, no. 5, pp. 423–442, 2006.

[25] H. L. Corrêa, A. M. F. De Sousa, and C. R. G. Furtado, "Natural rubber latex: Determination and interpretation of flow curves," *Polimeros*, vol. 25, no. 4, pp. 365–370, 2015.

[26] W. V. Titow, *PVC Plastics: Properties, Processing and Applications*, 6th ed. London, U.K.: Science, 1990.

[27] A. Sommerfield, "Ein Beitrag zur hydrodynamischen Erklarung der turbulenten Flus-sigkeisbewegung," in *Proc. 4th Atti Congr. Int. Math.*, vol. 3, 1908, pp. 116–124.

[28] J. C. Lagarias, J. A. Reeds, M. H. Wright, and P. E. Wright, "Convergence properties of the Nelder-mead simplex method in low dimensions," *SIAM J. Optim.*, vol. 9, no. 1, pp. 112–147, 1998.

[29] P. N. Kakar, J. Das, P. M. Roy, and V. Pant, "Robotic invasion of operation theatre and associated anaesthetic issues: A review," *Indian J. Anaesthesia*, vol. 55, no. 1, pp. 18–25, 2011.

[30] R. Fuhrer, C. M. Schumacher, M. Zeltner, and W. J. Stark, "Soft iron/silicon composite tubes for magnetic peristaltic pumping: Frequency-dependent pressure and volume flow," *Adv. Functional Mater.*, vol. 23, no. 31, pp. 3845–3849, 2013.